Chemical analysis of actinolite from reflectance spectra

John F. Mustard

Department of Geological Sciences, Box 1846, Brown University, Providence, Rhode Island 02912, U.S.A.

Abstract

Reflectance spectra of medium (0.005 μm between 0.3 and 2.7 μm) and high (0.0002 μm between 1.38 and 1.42 μm and 0.002 μm between 2.2 and 2.5 μm) spectral resolution of 19 minerals from the tremolite-actinolite solid solution series are used to characterize systematic variations in absorption band parameters as a function of composition. The medium-resolution data are used to characterize broad absorptions associated with electronic processes in Fe^{3+} and Fe^{2+}, and the high-resolution data are used to characterize overtones of OH vibrational bands. Quantitative analyses of these data were approached using a model that treats absorptions as modified Gaussian distributions (Sunshine et al., 1990). Each spectrum was deconvolved into a set of additive model absorption bands superimposed on a reflectance continuum. For absorptions associated with electronic processes, the model bands were shown to provide estimates of the Fe and Mg mineral chemistry with correlations of greater than 0.98. The systematic changes in the energy, width, intensity, and number of OH overtone bands are easily quantified using the modified Gaussian model, and the results are highly correlated with the Fe/Mg ratios of the samples. These results indicate that the modified Gaussian model can be used to quantify objectively the bulk chemistry of the minerals of the tremolite-actinolite solid solution series using high-resolution reflectance spectra of the OH overtone bands.

Introduction

Extraction of quantitative geochemical information is an important goal in reflectance spectroscopy, both as a tool for rapid and nondestructive laboratory analyses and for interpretation of remotely obtained observations of the Earth and other solid bodies in the solar system. The chemical and crystallographic bases for the interpretation of absorption bands in reflectance spectra are reasonably well understood (e.g., Burns, 1970; Farmer, 1974; Hunt, 1977). The assignment of a particular absorption to a specific crystallographic site geometry and absorbing species have proven consistent across a large range of compositions and crystal structures. This knowledge has been extremely valuable for the remote identification of mineral species on other planets (e.g., Pieters, 1986; McCord et al., 1982). However, there have been few detailed analyses to determine quantitative associations between the position, shape, and strength of absorption bands in reflectance spectra and the chemical composition of minerals. A sound understanding of the relationship between absorption band parameters and specific mineral chemistry would have a broad range of applications in the reduction and analysis of remotely obtained and laboratory reflectance spectra.

One desires a method of deconvolving reflectance spectra into concentrations of absorbing species that produces quantitative results and is general in approach. Sunshine et al. (1990) have made some progress in this area by deconvolving Fe^{2+} absorptions in pyroxenes and olivines into realistic probability distributions. In the analyses presented here, a similar approach is applied to the absorptions associated with electronic and vibrational processes in calcic amphiboles and, more specifically, the minerals of the tremolite-actinolite-ferroactinolite solid solution series. Calcic amphiboles are very common in terrestrial geologic terranes, especially mafic and ultramafic terrane, and specific compositions often can be used to infer physical conditions of mineral and rock formation (e.g., Laird and Albee, 1981; Skogby and Annersten, 1985). The goal of this investigation is not only to model the specific absorptions associated with calcic amphiboles but also to provide insight into the absorption processes in general that can be used in the analysis of other minerals and mineral groups. Background discussions of actinolite crystal structure, chemistry, and absorption processes are presented below, followed by a detailed discussion of the modeling approach. The results of the modeling of the reflectance spectra are then presented with an emphasis toward the association between model parameters and sample chemistry.

Actinolite crystal structure and chemistry

Understanding of the variability of the reflectance spectra shown in Figure 1 requires a basic knowledge of crystal structure and chemistry. The idealized actinolite chemical formula, $Ca_2(Mg,Fe)_5Si_8O_{22}(OH)_2$, is rarely encountered with natural samples. There are generally appreciable amounts of Al^{3+}, Fe^{3+}, Mn, Cr, and Na in these
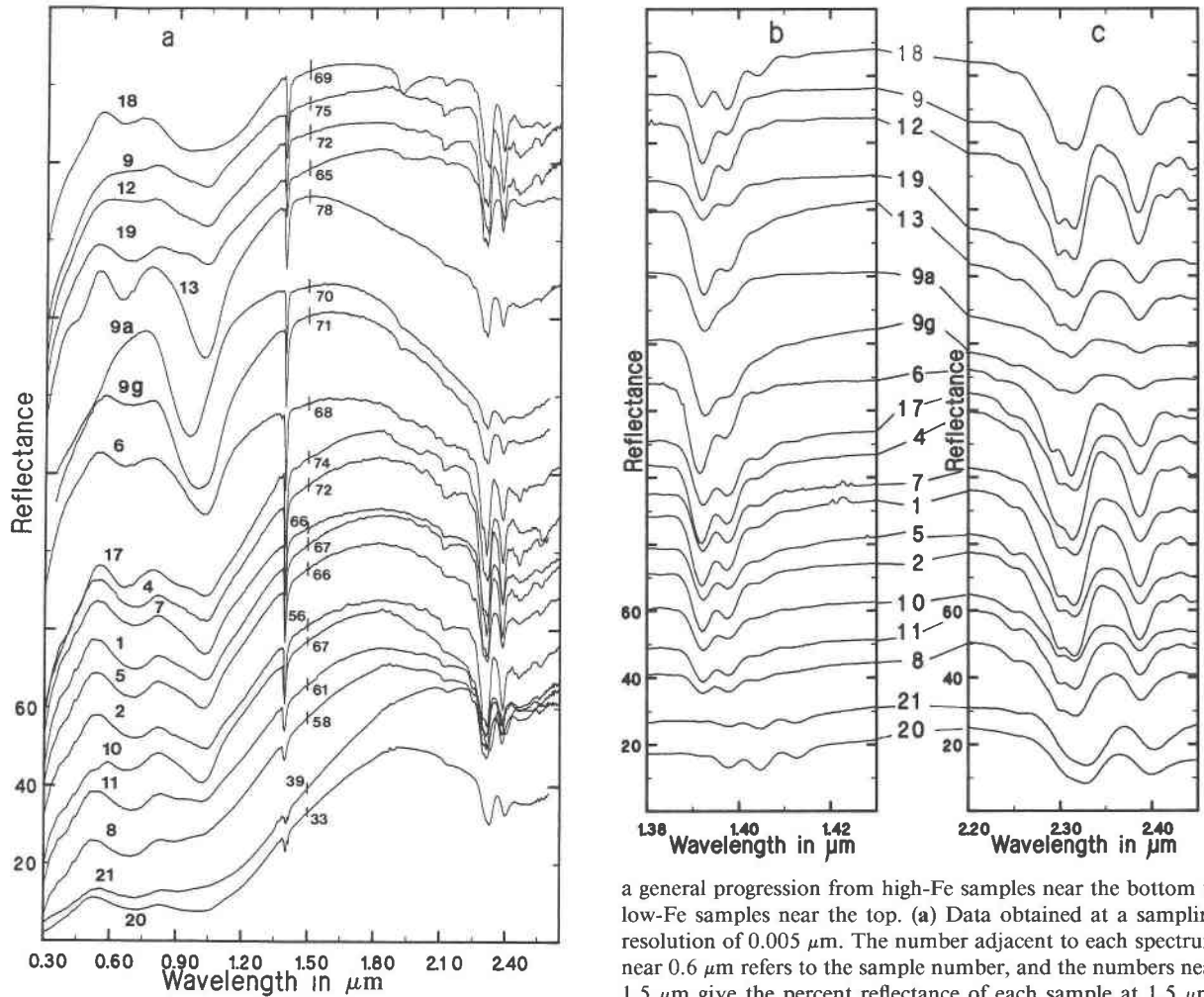
Fig. 1. Reflectance spectra of 19 samples from the tremolite-actinolite solid solution series. All data have been offset for clarity approximately 5% relative to each other. The numbers on the left side of each plot indicate the reflectance scale. There is a general progression from high-Fe samples near the bottom to low-Fe samples near the top. (a) Data obtained at a sampling resolution of 0.005 μm. The number adjacent to each spectrum near 0.6 μm refers to the sample number, and the numbers near 1.5 μm give the percent reflectance of each sample at 1.5 μm. (b) Reflectance spectra obtained at a sampling resolution of 2 Å between 1.38 and 1.43 μm; (c) data obtained at a sampling resolution of 0.002 μm between 2.2 and 2.45 μm. The numbers between b and c indicate the sample number of the spectra joined by the solid lines.

minerals. The actinolite crystal structure is monoclinic with space group $C2/m$ and consists of two unique tetrahedral sites (T1, T2), four unique octahedrally coordinated sites (M1, M2, M3, and M4), and one 12-coordinated site (A) (Ghose, 1961).

Site populations are complex in amphiboles (see Hawthorne, 1983, for a review) and are important for the interpretation and quantification of actinolite reflectance spectra. Al^{3+} shows a site preference for T1 when in tetrahedral coordination and the M2 site when in octahedral coordination. Fe^{3+}, like Al^{3+}, exhibits a preference for the M2 site (Wilkens, 1970; Hawthorne, 1983; Skogby and Annersten, 1985). However, local charge balance can influence these general distributions. Although Fe^{2+} can occupy any of the four octahedral sites and the specific ordering among these sites is complex, several studies have

shown that Fe^{2+} is enriched in M1 and M3 relative to M2 in calcic amphiboles (Burns and Prentice, 1968; Ernst and Wai, 1970; Wilkens et al., 1970; Wilkens, 1970). Mg shows a site preference that is complementary to Fe^{2+}. Ca almost exclusively occupies the M4 site, but there is rarely enough Ca to fill this site completely. Vacant M4 sites are preferentially filled by available Mn and Fe^{2+}.

Sources of absorption in calcic amphiboles

Three basic processes are responsible for the suite of absorptions observed in the spectra shown in Figure 1. Excitation of d-orbital electrons in transition metal ions, particularly Fe, is primarily responsible for the broad absorptions centered between 0.85 and 1.2 μm. The broad absorption centered near 2.45 μm is largely due to an electronic transition. Absorptions involving transfer of

electrons between anions and cations generally exhibit band minima at wavelengths less than about 0.5 μm, but wings of these absorptions do extend through the visible to the near infrared. Cation-to-cation charge transfer absorptions can have well-defined visible to near infrared absorptions. Finally, overtones and combination overtones of fundamental vibrational bands associated with OH ions account for the narrow features near 1.4 μm and at wavelengths longer than 2.0 μm. Details of each category of absorption and relationship to cation and anion site occupancy are discussed below.

Electronic transitions. The energy of electronic transition absorptions is determined by the crystal field splitting, whereas the intensity or strength of the absorptions is governed by probability considerations determined primarily by site distortion and symmetry (Burns, 1970; White and Keester, 1967). The broad, indistinct absorptions between 0.85 and 1.2 μm are generally assigned to Fe^{2+} electronic transitions in M1, M2, and M3 (Hawthorne, 1981). However, little has been done to quantify further the exact assignment of these bands because these three sites are so similar in general size and shape that individual electronic transitions in these sites are probably not resolvable. Goldman and Rossman (1977) demonstrated that Fe^{2+} in the M4 site is primarily responsible for the deep, well-resolved 1.0- and 2.4-μm bands observed in transmission spectra of actinolite and tremolite. These absorptions are extremely intense because the M4 site is very distorted and lacks a center of symmetry. Although Ca and Mn occupy this site with greater efficiency than Fe^{2+}, Goldman and Rossman (1977) interpret the results as indicative of a strong preference of Fe^{2+} for this site. Other ions that exhibit absorptions due to electronic transitions in this wavelength region are Fe^{3+}, Cr^{3+}, and Mn^{2+}. In the data shown in Figure 1, the weak, narrow features between 0.3 and 0.6 μm are due to spin-forbidden electronic transitions in Fe^{2+} and Fe^{3+}. Cr^{3+} absorptions are observed in spectrum 13, shown in Figure 1a, and are centered near 0.45 and 0.6 μm.

Charge transfer. For the actinolite samples studied here the predominant intervalence charge transfer absorptions are between Fe^{2+} and Fe^{3+}. These account for the absorptions of variable intensity centered between 0.6 and 0.8 μm. For charge transfer absorptions to occur, the ions must be in adjacent crystallographic sites, either edge- or face-shared polyhedra, and the direction of separation between the sites must be parallel to the electronic vector of the incident radiation (Allen and Hush, 1967; Smith and Strens, 1976). Crystallographic arguments and Mössbauer analyses indicate that Fe^{3+} shows a preference for the M2 site. Since the M2 site shares at least one edge with the other three sites, this cation-to-cation absorption is expected to occur freely.

Vibrational bands. The sharp, narrow absorptions observed in the spectra shown in Figure 1b are overtones of the fundamental OH^- stretching absorptions that occur between 2.7 and 2.8 μm. The fundamentals have been the subject of many studies of calcic amphiboles (e.g.,

Burns and Strens, 1966; Bancroft and Burns, 1969; Wilkens, 1970; Burns and Greaves, 1971; Law, 1976). The wavelength position of the OH^- stretching fundamental depends on the cation occupancy of the two M1 and one M3 sites as a unit. For an ideal actinolite solid solution, there are four unique distributions: A = (MgMgMg), B = (MgMgFe), C = (FeFeMg), and D = (FeFeFe). Since each results in a distinct absorption, there are four possible OH^- stretching fundamentals in a simple Fe-Mg amphibole system. Additional bands can be expected if the M1 and M3 sites are occupied by other ions (e.g., Al^{3+}, Fe^{3+}) or the A site is occupied by Na or K.

The narrow absorptions between 2.2 and 2.5 μm (see Figs. 1a and 1c) are combination overtones involving OH^- stretching vibrations and metal-OH^- bending modes (Hunt, 1977). Although the location of the fundamental metal-OH^- bending modes is reasonably well known (500–800 cm^{-1} or 12–15 μm), there has been little work to quantify relationships between parameters that characterize absorption and chemistry or crystal structure. An increase in the wavelength position of the fundamental bending modes with increasing Fe content has been observed by Kukovskii and Litvin (1970) and Barabanov et al. (1974).

Approach to quantitative analysis

The general systematics of the reflectance relative to composition are simple. Samples with the most Fe^{2+} (21, 20, and 8) have deeper and broader absorptions between 0.8 and 1.2 μm relative to samples with the least Fe^{2+} (9 and 12), and samples with abundant Fe^{3+} (e.g., 8, 19, and 21) exhibit more intense charge transfer absorptions relative to samples with little Fe^{3+} (9a, 9, and 12). However, the association between absorptions and chemical composition in reflectance spectra has been difficult to quantify. Some success has been achieved in simple solid solution series like pyroxenes (Adams, 1974; Hazen et al., 1978) and olivines (Hazen et al., 1977; King and Ridley, 1987) relating band minima and band areas to chemistry. The complex substitution and number of unique absorbing sites in the minerals of the tremolite-ferroactinolite series preclude the use of such simple characterizations of absorptions. Investigators have modeled crystal field absorptions assuming that the absorptions have a Gaussian distribution in energy (Smith and Strens, 1976; Farr et al., 1980; Clark, 1981; Roush and Singer, 1986; Huguenin and Jones, 1986). However, these applications required two overlapping bands to model adequately absorptions thought to be the result of a single electronic transition, and they failed to produce results that could be related to composition.

Sunshine et al. (1990) have critically evaluated the use of Gaussians to model electronic transitions and have proposed a modified Gaussian model (MGM). The physical basis of this model is as follows. The energy potential of any absorbing ion in a given site can be approximated as a harmonic oscillator when perturbed by photon interactions. A harmonic oscillator has a Lorentzian distri-

bution in energy because of exponential damping in the time domain. However, absorption bands in reflectance spectra are due to photon interactions with millions of unit cells that, because of crystal defects, vacancies and substitutions, and thermal vibrations, have a Gaussian distribution of bond lengths about a mean. Therefore bond length is a random variable. Since bond length determines the energy of absorption, a Gaussian distribution of bond lengths will result in a statistical distribution of absorption energies. The key parameter to determine is the mathematical description of the distribution of absorption energies.

Sunshine et al. (1990) modeled absorptions in transmission and reflectance spectra of clino- and orthopyroxene with a Gaussian equation. These pyroxenes exhibit two dominant electronic transition absorptions, one near 1.0 μm and the other near 2.0 μm. Since each absorption is thought to be due to a single electronic transition (Burns, 1970), any realistic model should require only one band to describe each absorption. The classical Gaussian model of band shape required two overlapping bands to model these single absorptions, and the results failed to produce any correlations with chemistry. Crystal field theory states that the energy of electronic absorptions is proportional to cation-anion bond length raised to the nth power (Burns, 1970; Marfunin, 1979). Therefore Sunshine et al. (1990) modified the Gaussian equation to include an exponent for the energy term. They empirically determined the best value for the exponent as -1 by fitting single electronic absorptions in orthopyroxene. The same exponent also applies to single electronic absorptions in clinopyroxene. From this relationship it is inferred that the potential energy of a site is dominated by the Coulombic potential energy.

The results of Sunshine et al. (1990) indicate that the MGM is a significant advance over previous modeling approaches for reflectance spectra. The model was applied successfully to pyroxene mineral mixtures to determine end-member concentrations (Sunshine and Pieters, 1991), to characterize olivine composition in the forsterite-fayalite solid solution series (Sunshine and Pieters, 1990), and to separate the end-member reflectance spectra of mineral components in an intimate mixture (Mustard, 1991). In the analyses presented here, the MGM model is used to characterize the complex overlapping electronic transition and charge transfer absorptions in low-resolution spectra and the overtone and combination overtone OH absorption in high-resolution spectra of actinolite. Although the MGM model was not developed specifically to model OH or charge transfer absorptions, the general principles behind the MGM model apply.

EXPERIMENTAL PROCEDURES

Samples

Sixteen samples that can be reasonably assigned to the tremolite-actinolite-ferroactinolite solid solution series were acquired for analysis of the spectral and chemical properties. The samples were inspected under an optical microscope for homogeneity. Major element oxide concentrations, presented in Table 1, were measured with the microprobe facility at Brown University. TiO$_2$ content was also measured but is not reported in Table 1, since the concentration of this oxide was always at or below the sensitivity limits of the microprobe (0.01%). Fe^{2+} content was analyzed by volumetric microtitration (Thornber et al., 1980). Fe^{3+} content was then calculated from the total Fe analyzed by the microprobe using simple mass balance:

$$Fe_2O_3 = (FeO_{probe} - FeO_{titration}) \times 1.1113.$$

Two titrations were performed on each sample and were averaged (Skoog and West, 1982). An evaluation of the uncertainty in titrations was made using laboratory standard material TRS138-9D2 (supplied by J. G. Schilling of the University of Rhode Island). Five samples of the standard titrated with each batch of unknowns yielded an average value of 7.67 ± 0.12 wt% FeO (accepted value 7.75 wt% FeO, Gwinn and Hess, 1989). An additional three actinolite samples were loaned by R. G. Burns for measurement of the spectral properties. Chemical analyses of these samples were performed elsewhere, and references for these analyses are given in Table 1. Based on these general site preferences and the method of Robinson et al. (1982), the oxide concentrations are cast into site occupancy assignments in Table 1. These site assignments and populations are approximate, and precise determinations require detailed and coordinated Mössbauer, X-ray, and infrared techniques.

Bidirectional reflectance spectroscopy

All reflectance spectra used in this analysis were obtained with the RELAB spectrometer, a high-resolution bidirectional spectrometer at Brown University supported by NASA as a multiuser facility. RELAB is designed to obtain reflectance measurements at specific angles of incidence and emergence, defined by the user, to simulate geometries used in the acquisition of data by instruments on spacecraft, aircraft, and telescopes. These unique capabilities also permit the investigation of the angular distribution of light due to scattering, transmission, and reflection off a surface. Detailed descriptions of the instrument are given by Pieters (1983) and Mustard and Pieters (1989). Briefly, a beam of monochromatic light is focused on the sample at a specific angle of incidence between 0 and 60° to the surface normal. The reflected radiation is detected using a cooled photomultiplier tube for ultraviolet to visible wavelengths and an indium-antiminide detector for longer wavelengths, at emergence angles between -60 and 60°. RELAB has a practical operating wavelength range of between 0.3 and 3.7 μm with an average spectral resolution of 3.2 nm. The instrument precision is better than 0.25%, which is smaller than potential systematic error due to diffraction or sample preparation. Raw data are normalized to measurements obtained simultaneously of pressed halon, an inert

fluorocarbon that is uniformly bright between 0.25 and 2.7 μm. These relative reflectance data are then calibrated to absolute reflectance using the calibration factors for halon given by Weidner and Hsia (1981).

Samples were measured at 5-nm sampling resolution between 0.3 and 2.7 μm, at 2-Å sampling resolution between 1.35 and 1.45 μm, and at 2-nm sampling resolution between 2.2 and 2.5 μm. The low-resolution spectral data (5 nm) are used to characterize broad absorptions associated with electronic processes, whereas the high-resolution data (2 Å, 2 nm) are used to characterize the sharp, narrow absorptions associated with vibrational processes. A standard viewing geometry with an incidence angle of 30° and emergence angle of 0° was used in all measurements. The samples were ground with a mortar and pestle to enhance the intensity of spectral features. Since the total amount of some samples was very limited, no attempt was made to isolate a particular grain-size fraction. The particle diameters of the samples are in general less than 250 μm in size with a sizeable fraction of the particles less than 30 μm. About 1 g of sample was required to fill the sample dishes, which were 1 cm in diameter by 5 mm deep. Low-resolution, full wavelength spectra are shown in Figure 1a, high-resolution spectra of the 1.38–1.43 μm region are shown in Figure 1b, and high-resolution spectra of the 2.2–2.5 μm region are shown in Figure 1c.

Modified Gaussian model and modeling approach

The MGM of Sunshine et al. (1990) states that for a given absorption with position (μm) there is a distribution in energy (x) with a standard deviation (σ) and amplitude (s). This is given by the equation

$$m(x) = s \exp[-(x^{-1} - \mu^{-1})^2/2\sigma^2]$$

where $m(x)$ is the modified Gaussian expressed as a function of energy. In reflectance spectra, as in transmission spectra, absorption obeys the Beer-Lambert law. To establish a linear system of additive, overlapping absorptions the reflectance data are first converted to natural log reflectance, and the dependent variable is energy (cm^{-1}). However all data and results will be presented as a function of wavelength for consistency and clarity. The effects of multiple scattering, Fresnel reflectance, and low-energy wings of strong metal-O charge transfer absorptions in the ultraviolet are partially modeled by a straight line continuum in energy. The model distributions are superimposed on this continuum.

A nonlinear least-squares algorithm developed by Kaper et al. (1966) is used to determine MGM solution to the spectra. This algorithm permits simultaneous analysis of the entire spectrum. Initial conditions for each band (position, width, strength) and the continuum are provided, and the fitting procedure incrementally adjusts the model parameters until possible improvement in fit is negligible. The number of bands selected for initial parameters is determined from inspection of the reflectance spectra for resolved band minima and inflections. The
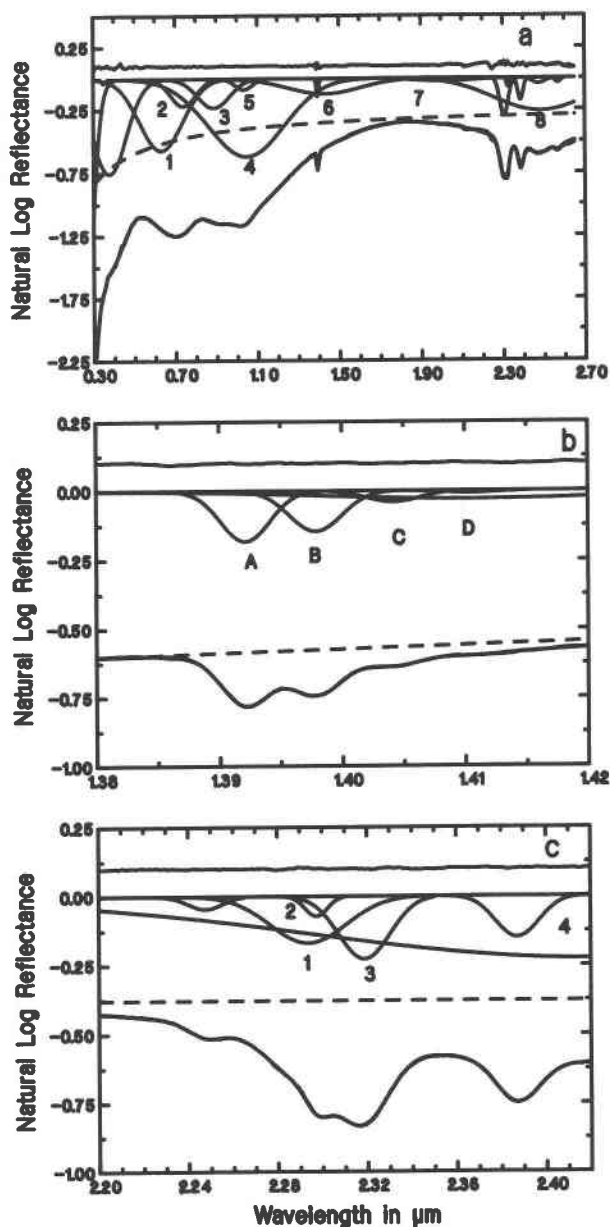
Fig. 2. Representative MGM solutions applied to sample 11 for each of the spectral sampling resolutions. The solutions are presented in natural log reflectance since the calculations are carried out in these units. In each plot the measured and predicted spectra are shown as solid lines, and the residual spectrum (data model) is shown as the solid line near the top of each plot. The continuum is the dashed line. (a) A total of 18 model bands are required to attain the MGM solution. The eight numbered bands are interpreted to model the well-resolved electronic transition and charge transfer absorptions. (b) The four labeled bands A, B, C, and D correspond the metal-OH stretching models of the same designation presented by Burns and Strens (1966). An additional unlabeled band models absorption due to absorbed H_2O. (c) The four model bands that are most strongly correlated with mineral chemistry are labeled 1–4.

TABLE 1. Chemical analyses of actinolite

Sample	1	2	4	5	6	7	8	9	10	11	12	13
					Oxide percentages							
SiO_2	56.61	56.34	56.22	55.31	56.84	56.21	52.45	57.81	56.45	55.43	58.15	54.86
Al_2O_3	1.01	0.88	0.83	2.27	1.14	0.80	5.27	0.46	1.62	2.24	0.27	3.52
Fe_2O_3	1.95	1.70	2.62	0.41	0.43	0.60	3.36	0.27	0.38	0.62	0.23	0.58
FeO	3.72	3.98	3.49	4.67	2.47	5.70	7.45	2.65	5.55	5.39	2.41	4.13
MgO	20.24	20.75	20.80	20.80	22.87	20.66	17.43	23.35	21.77	20.78	23.52	20.98
CaO	12.91	13.01	13.16	12.75	12.05	12.61	11.79	13.63	12.21	12.74	13.53	11.83
MnO	0.37	0.28	0.31	0.29	0.11	0.11	0.53	0.29	0.34	0.34	0.31	0.16
Cr_2O_3	0.16	0.31	0.03	0.03	0.13	0.13	0.38	0.04	0.29	0.12	0.02	1.53
Na_2O	0.32	0.27	0.27	0.28	0.76	0.19	1.07	0.22	0.37	0.43	0.18	0.74
K_2O	0.03	0.02	0.03	0.02	0.01	0.04	0.07	0.13	0.04	0.03	0.10	0.07
Total	97.32	97.54	97.76	96.83	96.81	97.05	99.80	98.85	98.94	98.12	98.72	98.40
					Cations per formula unit							
Si	7.844	7.842	7.814	7.746	7.864	7.881	7.318	7.870	7.760	7.702	7.907	7.568
Al	0.166	0.144	0.136	0.375	0.186	0.132	0.867	0.074	0.262	0.367	0.043	0.572
Fe^{3+}	0.204	0.178	0.274	0.043	0.045	0.063	0.353	0.028	0.039	0.065	0.024	0.060
Fe^{2+}	0.433	0.463	0.406	0.547	0.286	0.668	0.869	0.302	0.638	0.626	0.274	0.477
Mg	4.202	4.306	4.310	4.343	4.717	4.318	3.626	4.739	4.461	4.305	4.768	4.315
Ca	1.926	1.940	1.960	1.913	1.786	1.894	1.763	1.988	1.798	1.879	1.971	1.749
Mn	0.044	0.033	0.036	0.034	0.013	0.013	0.063	0.033	0.030	0.040	0.036	0.019
Cr	0.018	0.034	0.003	0.003	0.014	0.014	0.042	0.004	0.032	0.013	0.002	0.167
Na	0.086	0.073	0.073	0.076	0.204	0.052	0.289	0.058	0.099	0.116	0.047	0.198
K	0.005	0.004	0.005	0.004	0.002	0.007	0.012	0.023	0.007	0.005	0.017	0.012
					Estimated site populations							
Si(T)	7.88	7.84	7.81	7.75	7.86	7.88	7.32	7.87	7.76	7.70	7.91	7.57
Al(T)	0.12	0.14	0.14	0.25	0.14	0.12	0.68	0.07	0.24	0.30	0.04	0.43
Fe^{3+}(T)	0.00	0.02	0.05	0.00	0.00	0.00	0.00	0.03	0.00	0.00	0.02	0.00
Al(M123)	0.05	0.00	0.00	0.12	0.05	0.01	0.19	0.00	0.01	0.07	0.00	0.14
Fe^{3+}(M123)	0.20	0.16	0.22	0.04	0.04	0.06	0.35	0.00	0.04	0.06	0.00	0.06
Cr(M123)	0.02	0.03	0.00	0.00	0.01	0.01	0.04	0.00	0.03	0.01	0.00	0.17
Mg(M123)	4.20	4.31	4.31	4.34	4.72	4.32	3.63	4.75	4.46	4.30	4.77	4.31
Fe^{2+}(M123)	0.43	0.46	0.41	0.50	0.18	0.60	0.79	0.25	0.46	0.56	0.23	0.32
Mn(M123)	0.04	0.03	0.04	0.00	0.00	0.00	0.00	0.00	0.00	0.00	0.00	0.00
Fe^{2+}(M4)	0.00	0.00	0.00	0.05	0.11	0.07	0.08	0.05	0.18	0.07	0.04	0.12
Mn(M4)	0.00	0.00	0.00	0.00	0.00	0.00	0.06	0.03	0.03	0.04	0.04	0.02
Ca(M4)	1.93	1.94	1.96	1.91	1.79	1.89	1.76	1.92	1.79	1.89	1.92	1.75
Na(M4)	0.07	0.06	0.04	0.04	0.10	0.04	0.10	0.00	0.00	0.00	0.00	0.11
Ca(A)	0.00	0.00	0.00	0.00	0.00	0.00	0.00	0.07	0.01	0.01	0.05	0.00

Note: Sample origins: 1, 2, and 6 = Brown Teaching Collection; 4 = Oaklawn, RI; 5 = Smithfield, RI; 8 = West Cummington, MA; 9 = Warren County, NJ; 10 = Cumberland, RI; 11 = Chester, VT; 12 = Lee, MA; 13 = Lake Heneteh; 17 = Orange County, CA; 18 = Cassiar, B.C., Canada; 19 = no. 14785 Berkeley, CA; 20 = Mueller 12ba, Quebec; 21 = USNM 44973, Cumberland, RI; 9a, 9g = Porterville, CA. All chemical analyses conducted at Brown University except 19 (from Burns and Greaves, 1970), 20 (from Mueller, 1960), and 21 (from Mitchell et al., 1970).

need for additional bands is indicated in the residual spectrum by a characteristic sinusoidal shape. The implementation of the Kaper et al. (1966) algorithm allows for selective toggling of band parameters to constrain solutions (e.g., band width of OH overtone absorptions) and assist in deriving solutions in complex systems of overlapping bands.

The MGM was applied to each of the spectra shown in Figure 1. Two criteria are used to determine when an adequate solution is achieved: (1) The total error of the fit is within a few tens of percent of the measurement error (0.25%). (2) There are no systematic errors as a function of wavelength. Initially a complex spectrum was fitted iteratively, adding new bands until a residual error (data model) satisfying criterion 1 was obtained. The minimum number of bands required to satisfy the second criterion has been used. The general shape and relative position of these bands are then used as initial starting parameters for each of the remaining spectra. Each suite of spectra is treated separately, and representative model solutions for sample 11 are shown in Figure 2 for each of the wavelength resolutions.

Low-resolution data. A total of 18 bands are required to attain a reasonable fit to all features (Fig. 2a). Seven are used for the OH bands, and three are used to fit the edge of the ultraviolet absorption between 0.3 and 0.55 μm. The remaining eight bands, labeled 1–8 in Figure 2a, model the resolved charge transfer and electronic transition absorptions. Ideally each band should be associated with a specific absorbing species in a specific site. However, since the three octahedral sites M1, M2, and M3 are almost identical in size, we can anticipate a high degree of overlap in the Fe^{2+} crystal field absorptions from these sites. Some of the model bands are almost certainly combinations of electronic transitions from several sites. Nevertheless, they provide a consistent set of parameters for understanding the relationship between chemistry and absorption in actinolite mineral spectra. Model parameters for the eight primary bands and the total error of the fit are presented in Table 2.

High-resolution OH overtones. The data in Figure 1b were fitted using band positions from Farmer (1974) and initially fixing band widths to lie between 6 and 10 cm⁻¹ (Burns and Strens, 1966; Burns and Greaves, 1971). An

TABLE 1—*Continued*

17	18	19	20	21	9a	9g
Oxide percentages						
57.09	57.45	56.00	55.00	50.61	57.05	56.45
0.65	0.26	2.30	0.60	2.42	0.45	1.50
0.27	0.01	1.40	1.83	2.80	0.10	0.41
5.80	4.96	4.22	19.60	19.90	5.46	5.01
20.65	21.76	20.00	11.00	8.26	2.61	22.00
12.24	13.22	11.10	10.00	10.82	1.58	11.90
0.33	0.29	0.11	0.29	2.69	0.22	0.29
0.30	0.15	—	—	—	0.03	0.24
0.62	0.03	1.10	0.24	0.48	0.07	0.08
0.05	0.02	0.10	0.01	0.14	0.01	0.04
98.00	98.15	96.34	98.58	98.13	97.58	97.92
Cations per formula unit						
7.927	7.932	7.848	8.051	7.655	7.905	7.803
0.106	0.042	0.380	0.104	0.431	0.073	0.244
0.028	0.001	0.148	0.202	0.319	0.010	0.043
0.673	0.573	0.495	2.399	2.517	0.633	0.579
4.274	4.479	4.178	2.400	1.863	4.671	4.534
1.821	1.956	1.667	1.568	1.754	1.719	1.762
0.039	0.034	0.013	0.036	0.345	0.026	0.034
0.033	0.016	—	—	—	0.003	0.026
0.167	0.008	0.299	0.068	0.141	0.019	0.021
0.009	0.004	0.018	0.002	0.027	0.002	0.007
Estimated site populations						
7.93	7.93	7.85	8.05	7.66	7.91	7.80
0.07	0.04	0.15	0.00	0.34	0.07	0.20
0.00	0.03	0.00	0.00	0.00	0.01	0.00
0.04	0.00	0.23	0.10	0.09	0.00	0.04
0.03	0.02	0.15	0.20	0.32	0.00	0.04
0.03	0.02	0.00	0.00	0.00	0.00	0.03
4.27	4.48	4.18	2.40	1.86	4.67	4.53
0.63	0.49	0.42	2.30	2.52	0.33	0.36
0.00	0.00	0.00	0.00	0.21	0.00	0.00
0.04	0.04	0.06	0.10	0.00	0.30	0.22
0.04	0.03	0.01	0.04	0.13	0.03	0.03
1.82	1.92	1.67	1.57	1.75	1.67	1.75
0.10	0.00	0.26	0.07	0.12	0.00	0.00
0.00	0.03	0.00	0.00	0.00	0.05	0.01

Fig. 3. Oriented single crystal transmission spectra of actinolite from Goldman and Rossman (1977). The α spectrum (solid line) was measured parallel to the **a** axis, the β spectrum (dotted line) parallel to the **b** axis, and the γ spectrum (dashed line) parallel to the **c** axis. Transmission spectra can resolve absorptions that are superimposed and overlapping in reflectance spectra of particulate surfaces. Note the two resolved Fe^{3+}-Fe^{2+} charge transfer absorptions near 0.7 μm.

High-resolution combination overtones. The data in Figure 1c were fitted using a continuum and six bands (Fig. 2c). The continuum is a straight, horizontal line to provide a base for the bands, five bands are used to fit the well-resolved vibrational bands, and one band is used to approximate the contribution due to the electronic transition band. The four bands that are most highly correlated with composition are numbered. As with solutions to the overtone region of the stretching fundamentals, the model converges rapidly and consistently to a solution. Model parameters for the four primary bands and the total error of the fit are presented in Table 4.

RESULTS

Low-resolution data

The position, strength, and width of the model bands were compared with published polarized transmission spectra of actinolite (Burns, 1970; Goldman and Rossman, 1977; Hawthorne, 1981). Polarized transmission spectra of oriented samples can resolve bands that overlap and are superimposed in reflectance spectra. Transmission spectra of actinolite, reproduced from Goldman and Rossman (1977), are shown in Figure 3. Comparison of the model bands shown in Figure 2a with the transmission spectra shown in Figure 3 indicates a qualitative agreement in the number and position of absorptions and bands.

Bands 1 and 2 model the Fe^{2+}-Fe^{3+} charge transfer absorptions. Fe^{3+} shows a preference for the M2 site, which shares an edge with all three other sites. However, the positions of the M2 and M4 sites are probably too far apart, relative to the distance between the center of the M2 site and the M1 and M3 sites, to be much of a factor. It is unknown whether a given band (1 or 2) is uniquely

additional broad and shallow band was included to accommodate a diffuse absorption near 1.43 μm, probably due to adsorbed H_2O (Burns and Greaves, 1971). The continuum is a straight line segment tangent to the spectra on either side of these absorptions (Fig. 2b). Since the positions and widths of the OH overtone absorptions are expected to be independent of chemistry in a binary system (Burns and Strens, 1966; Burns and Greaves, 1971; Wilkens, 1970), the widths and positions of bands A, B, C, and D were initially fixed and only the strengths were allowed to vary. The continuum as well as the position, strength, and width of the extra broad band were allowed to vary freely. Following initial convergence of the model, these constraints are relaxed to remove any remaining error (Fig. 2b). Using the overtone region to model the OH stretching absorption quantitatively allows the continuum and absorption due to adsorbed H_2O to be modeled with free parameters. This overcomes some of the criticisms of Law (1976) regarding this method of analysis for the fundamental region. Model parameters for the four primary bands and the total error of the fit are presented in Table 3.
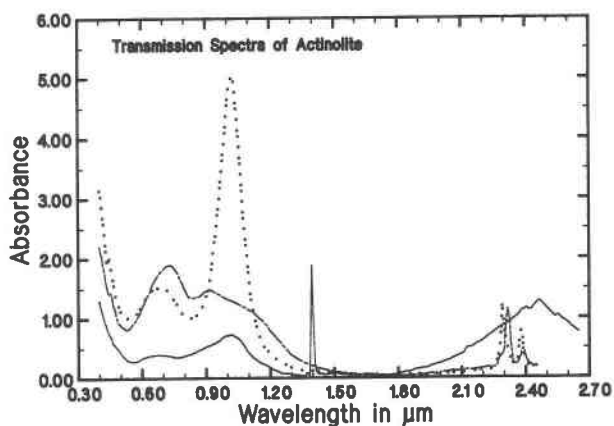
TABLE 2. Model parameters for electronic absorptions

Sample	1 Cen*	1 Wid**	1 Str†	2 Cen	2 Wid	2 Str	3 Cen	3 Wid	3 Str	4 Cen	4 Wid	4 Str
1	668.96	253.7	−0.474	742.25	129.8	−0.061	914.17	183.0	−0.135	1032.66	425.7	−0.592
2	656.97	248.1	−0.515	745.53	139.9	−0.112	908.31	185.3	−0.168	1032.66	425.7	−0.679
4	672.48	250.3	−0.391	731.27	111.0	−0.035	916.67	187.6	−0.083	1023.32	425.7	−0.558
5	651.20	237.8	−0.494	737.78	124.9	−0.112	894.33	195.4	−0.181	1031.24	430.2	−0.570
6	617.01	103.8	−0.029	686.61	157.9	−0.119	896.00	150.0	−0.075	992.92	378.0	−0.217
7	660.88	187.0	−0.302	752.10	118.0	−0.082	904.82	228.0	−0.168	1055.43	449.7	−0.442
8	619.04	254.0	−0.808	739.02	150.8	−0.308	880.59	175.5	−0.306	1030.45	436.7	−0.744
9	656.20	204.0	−0.107	742.53	100.2	−0.031	904.85	197.9	−0.063	1029.95	408.9	−0.272
10	652.97	246.9	−0.531	746.25	113.2	−0.061	908.63	187.1	−0.158	997.19	403.9	−0.480
11	631.36	247.2	−0.573	739.90	143.7	−0.221	887.45	182.1	−0.235	1046.41	436.8	−0.623
12	591.40	225.0	−0.113	722.68	150.0	−0.076	907.82	175.0	−0.037	1009.84	393.9	−0.250
13	617.01	103.8	−0.150	683.41	127.2	−0.166	977.10	146.4	−0.110	999.74	396.7	−0.353
17	658.34	217.9	−0.426	686.18	206.7	0.000	887.70	170.4	−0.112	1029.74	468.5	−0.583
18	629.81	99.3	−0.116	715.68	110.3	−0.091	878.37	175.0	−0.108	1048.23	423.7	−0.348
19	644.23	198.8	−0.251	739.38	159.4	−0.082	878.40	100.0	−0.030	977.49	415.8	−0.360
20	659.76	276.5	−1.432	770.62	142.9	−0.315	909.86	166.5	−0.581	1056.52	415.3	−1.312
21	656.79	300.1	−1.337	770.62	157.7	−0.257	909.86	165.4	−0.431	1056.52	454.2	−1.065
9a	585.99	179.0	−0.001	702.74	160.7	−0.001	809.55	380.6	−0.001	873.66	80.7	−0.056
9g	585.99	179.0	−0.120	702.74	160.7	−0.158	968.96	405.1	−0.336	1050.37	97.2	−0.055

* Center in nanometers.
** Width in nanometers.
† Strength in log absorptions.

associated with a particular site occupancy. The strength of charge transfer absorptions is thought to be proportional to the product of the concentration of donor and acceptor ions (Smith and Strens, 1976). The total area of bands 1 and 2 increases with the product of concentrations of Fe^{2+} and Fe^{3+} ions (Fig. 4). Although there is a monotonic increase in log area of absorption and the product of concentrations of Fe^{2+} and Fe^{3+}, it appears in Figure 4 that there is a rapid increase in band area at low values of the Fe^{2+}-Fe^{3+} concentration product, and the rate of increase in band area with increasing values of the Fe^{2+}-Fe^{3+} concentration product is less.

Bands 3 and 4 are interpreted here to model Fe^{2+} electronic transitions in the M1, M2, and M3 sites. Because the overall size and symmetry of these three sites are very similar, the magnitude of the d-orbital splittings and hence the energies and probabilities of absorption will be more or less equivalent. Also, since the electronic transitions in these sites are expected to occur between the equivalent energy levels, the widths of the absorptions will be comparable (Burns, 1970; Marfunin, 1979), and it will therefore be difficult to resolve individual absorptions with these data. The strength of band 5 is strongly correlated with the strength of band 8, with a correlation coefficient

TABLE 3. Model parameters for overtones of OH stretching absorptions

Sample	A Cen*	A Wid**	A Str†	B Cen	B Wid	B Str	C Cen	C Wid	C Str	D Cen	D Wid	D Str	Res % ref
1	1391.88	4.58	−0.4195	1397.62	5.09	−0.3212	1404.46	5.08	−0.0828	1412.49	5.09	−0.0212	0.0053
2	1392.14	4.55	−0.2861	1397.82	5.25	−0.2156	1404.35	5.08	−0.0610	1411.75	5.09	−0.0094	0.0060
4	1391.81	4.63	−0.5100	1397.60	4.70	−0.3713	1403.89	5.08	−0.1002	1409.80	5.09	−0.0229	0.0063
5	1392.14	4.55	−0.2861	1397.82	5.25	−0.2156	1404.35	5.08	−0.0610	1411.75	5.09	−0.0094	0.0060
6	1391.46	4.85	−0.4479	1397.31	4.94	−0.2423	1404.33	5.08	−0.0410	1411.48	5.09	−0.0100	0.0077
7	1396.12	4.50	−0.2988	1401.79	4.75	−0.2563	1408.25	5.08	−0.0710	1415.33	5.09	−0.0096	0.0080
8	1392.00	4.50	−0.1063	1397.91	5.49	−0.1084	1404.64	5.08	−0.0551	1411.44	5.09	−0.0279	0.0059
9	1392.14	4.62	−0.3344	1397.67	4.33	−0.1868	1403.29	5.08	−0.0261	1405.39	5.09	−0.0005	0.0037
10	1392.13	4.55	−0.2310	1397.79	5.25	−0.1646	1404.19	5.08	−0.0507	1410.52	5.09	−0.0105	0.0072
11	1396.13	4.55	−0.1810	1401.79	5.25	−0.1447	1408.19	5.08	−0.0424	1414.52	5.09	−0.0085	0.0027
12	1392.15	4.77	−0.3133	1397.76	4.29	−0.1688	1403.54	5.08	−0.0222	1412.32	5.09	−0.0006	0.0023
13	1396.23	4.58	−0.3215	1401.73	5.45	−0.2099	1408.19	5.08	−0.0469	1414.26	5.09	−0.0107	0.0033
17	1392.03	4.55	−0.3048	1397.66	5.25	−0.2591	1404.49	5.08	−0.0784	1411.63	5.09	−0.0165	0.0043
18	1391.88	4.60	−0.2407	1397.62	4.65	−0.2594	1404.24	5.08	−0.1008	1411.86	5.00	−0.0212	0.0040
19	1392.02	4.55	−0.1720	1397.69	5.25	−0.1117	1404.35	5.08	−0.0216	1411.67	5.09	−0.0031	0.0042
20	1395.61	4.55	−0.0304	1401.80	5.25	−0.1531	1408.79	5.08	−0.1916	1416.88	5.09	−0.1056	0.0049
21	1391.68	4.55	−0.0156	1397.93	5.25	−0.0673	1404.84	5.08	−0.1020	1412.84	5.09	−0.0761	0.0049
9a	1392.27	5.28	−0.2489	1397.64	5.94	−0.1218	1405.24	5.08	−0.0166	1410.84	5.09	−0.0104	0.0034
9g	1392.59	5.01	−0.5895	1397.99	4.89	−0.3648	1403.44	4.85	−0.0845	1409.48	5.09	−0.0080	0.0055

* Center in nanometers.
** Width in nanometers.
† Strength in log absorption.

TABLE 2—*Continued*

	5			6			7			8			Res
	Cen	Wid	Str	Cen	Wid	Str	Cen	Wid	Str	Cen	Wid	Str	% ref
1	1040.85	97.0	−0.133	1392.40	421.5	−0.093	2112.36	320.0	−0.035	2483.15	475.0	−0.314	0.0099
2	1042.62	90.6	−0.140	1392.40	421.5	−0.097	2090.00	320.0	−0.050	2486.23	475.0	−0.324	0.0093
4	1041.28	90.6	−0.103	1399.26	421.5	−0.083	2046.28	320.0	−0.044	2484.77	490.4	−0.374	0.0092
5	1034.01	106.8	−0.192	1394.18	401.7	−0.082	2136.80	358.1	−0.064	2485.12	473.0	−0.324	0.0079
6	1026.88	138.2	−0.273	1292.76	676.9	−0.059	2055.78	404.3	−0.140	2486.55	472.0	−0.475	0.0097
7	1037.97	108.2	−0.187	1511.65	367.7	−0.044	2070.19	395.3	−0.051	2484.63	475.0	−0.324	0.0055
8	1030.48	82.7	−0.053	1389.12	491.5	−0.204	2069.29	271.3	−0.023	2485.01	497.8	−0.225	0.0061
9	1042.62	90.0	−0.060	1313.62	671.7	−0.029	2071.87	343.9	−0.059	2485.77	400.0	−0.260	0.0071
10	1029.88	109.6	−0.199	1261.19	521.0	−0.170	2172.91	416.3	−0.078	2483.88	495.0	−0.384	0.0082
11	1033.86	97.1	−0.091	1429.02	417.8	−0.125	2056.51	368.9	−0.041	2487.91	485.0	−0.265	0.0077
12	1039.39	77.2	−0.049	1259.46	890.0	−0.074	2082.95	318.1	−0.076	2485.58	400.0	−0.260	0.0073
13	1031.62	115.4	−0.286	1230.45	601.1	−0.043	1889.10	460.0	−0.107	2467.15	700.3	−0.519	0.0060
17	1041.93	96.9	−0.098	1524.72	421.5	−0.060	2046.28	320.0	−0.044	2482.32	490.4	−0.374	0.0116
18	1041.08	150.0	−0.000	1344.19	784.1	−0.102	2030.26	556.5	−0.181	2484.74	400.0	−0.356	0.0082
19	1036.42	89.3	−0.086	1269.51	612.3	−0.099	2118.05	408.9	−0.050	2486.99	400.0	−0.260	0.0067
20	1039.40	113.1	−0.238	1376.23	612.0	−0.445	2083.71	272.7	−0.039	2483.76	484.1	−0.437	0.0084
21	1039.40	124.5	−0.093	1375.55	702.7	−0.516	2013.98	278.4	−0.014	2483.76	484.1	−0.188	0.0080
9a	960.65	168.1	−0.618	996.68	586.6	−0.145	1923.81	389.9	−0.062	2435.00	655.0	−0.728	0.0080
9g	989.73	194.6	−0.578	1192.39	449.3	−0.092	1857.42	250.0	−0.020	2477.10	738.4	−0.690	0.0082

of 0.94 (Fig. 5). The shape, position, correlated strengths, and relationship to the amount of Fe^{2+} in the M4 site (see Table 1) indicate that these two bands model the electronic absorptions associated with Fe^{2+} in the M4 site. This is the strongest assignment of model bands to specific electronic processes that can be made in this analysis.

Correlations between the log areas of MGM bands (total probability of absorptions) and major element contents were computed. Although there are weak linear trends between some band parameters and the amount

of Fe^{2+} per formula unit (pfu), no individual band is a sensitive indicator of the concentration of a specific element in the actinolite structure. This is not surprising since site populations and the relative strength of absorption bands are expected to be variable. From Beer's law, absorption is an exponential function of absorption coefficient. Therefore the log of absorption should be proportional to the concentration of the absorbing species in the site or sites responsible for the model band. It is apparent that the log area of band 5 is proportional to the amount of Fe^{2+} in the M4 site. If the log area of bands 3,

TABLE 4. Model parameters for combination overtones of OH absorptions

Sample	1			2			3			4			Res
	Cen*	Wid**	Str†	Cen	Wid	Str	Cen	Wid	Str	Cen	Wid	Str	% ref
1	2291.10	37.70	−0.3193	2297.74	13.16	−0.1608	2317.34	23.25	−0.4866	2386.36	22.72	−0.3159	0.0052
2	2290.68	38.43	−0.3743	2298.31	13.11	−0.1967	2317.70	23.50	−0.5735	2386.35	22.72	−0.3531	0.0040
4	2292.85	38.43	−0.5336	2296.29	13.11	−0.1066	2316.99	23.50	−0.6307	2386.03	22.72	−0.4031	0.0065
5	2294.22	38.43	−0.2156	2298.83	13.11	−0.0963	2318.96	23.50	−0.2816	2387.01	22.72	−0.1864	0.0030
6	2286.36	36.08	−0.2071	2289.81	13.32	−0.1899	2313.28	24.54	−0.5733	2386.13	24.86	−0.2541	0.0084
7	2286.37	38.43	−0.0593	2294.46	13.11	−0.0505	2313.49	23.50	−0.1418	2386.36	21.83	−0.0624	0.0021
8	2288.86	38.43	−0.2838	2297.95	13.11	−0.1625	2316.96	23.50	−0.4487	2386.55	22.72	−0.2322	0.0068
9	2292.50	38.43	−0.2131	2298.70	13.11	−0.1220	2318.47	23.50	−0.3323	2386.93	22.72	−0.2094	0.0024
10	2303.79	48.83	−0.1891	2297.33	8.34	−0.0287	2322.33	25.86	−0.0866	2388.42	22.72	−0.1098	0.0024
11	2282.71	28.27	−0.1796	2298.38	15.89	−0.2514	2316.67	20.82	−0.3797	2384.73	22.72	−0.2414	0.0053
12	2296.54	46.14	−0.1654	2297.63	11.29	−0.0590	2318.54	23.47	−0.1603	2386.77	22.72	−0.1237	0.0018
13	2293.74	39.97	−0.1698	2297.40	11.79	−0.0724	2318.78	26.83	−0.2288	2387.18	22.72	−0.1499	0.0019
17	2283.52	29.92	−0.1988	2298.27	15.19	−0.2439	2316.45	21.38	−0.4026	2384.70	21.84	−0.2404	0.0050
18	2288.80	38.43	−0.1225	2297.68	13.11	−0.0934	2316.61	23.50	−0.2234	2385.92	22.72	−0.1308	0.0018
19	2294.15	48.39	−0.2120	2298.26	12.92	−0.1053	2318.68	24.12	−0.2623	2386.52	22.72	−0.1923	0.0024
20	2294.01	43.50	−0.1972	2298.41	13.11	−0.0966	2319.49	25.68	−0.2755	2387.36	22.72	−0.1933	0.0028
21	2294.21	48.39	−0.1038	2297.71	12.92	−0.0547	2317.46	24.12	−0.1408	2386.47	22.72	−0.0864	0.0025
9a	2315.24	54.99	−0.2205	2304.74	18.56	−0.0346	2332.16	28.67	−0.1097	2399.13	36.93	−0.1423	0.0023
9g	2321.21	52.03	−0.2091	2304.24	17.51	−0.0288	2337.61	27.83	−0.0605	2403.36	37.10	−0.1306	0.0028

* Center in nanometers.
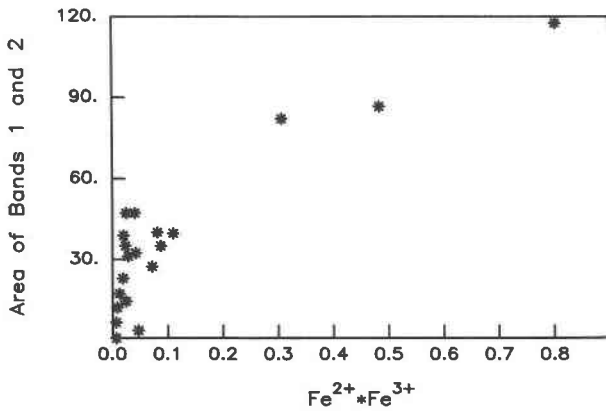** Width in nanometers.
† Strength in log absorption.

Fig. 4. The area of model bands 1 and 2 plotted against the product of Fe^{2+} and Fe^{3+} concentrations. Note the distinct increase in strength of these combined bands with increasing values of the product of Fe^{2+} and Fe^{3+} concentrations.
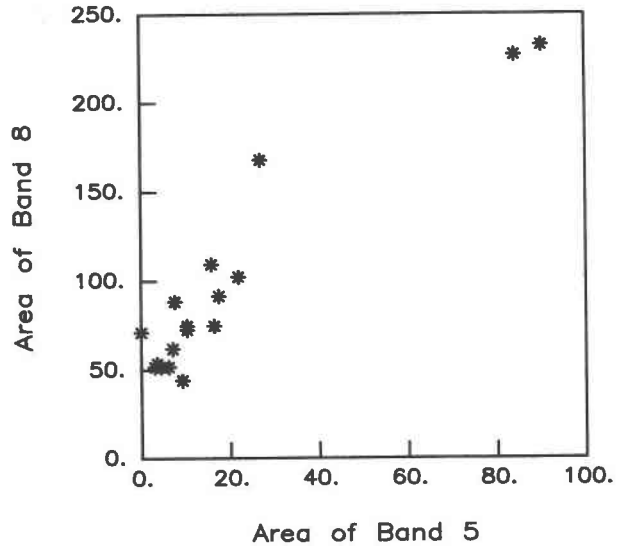

Fig. 5. The area of model band 8 plotted against the area of model band 5. These bands are interpreted to model Fe^{2+} electronic transitions in the M4 site (Goldman and Rossman, 1977), and the strongly positive correlation is consistent with this hypothesis.

4, and 6 is proportional to the amount of Fe^{2+} in the M1, M2, and M3 sites (or some combination of sites) then a linear equation relating band areas to sample chemistry can be established:

$$C_1 A_{b3} + C_2 A_{b4} + C_3 A_{b5} + C_4 A_{b6} + C_5 = Fe^{2+} \text{ pfu}$$

where C_1, C_2, C_3, and C_4 are proportionality coefficients for the log areas (A_b) of bands 3, 4, 5, and 6. The constant C_5 accounts for any systematic errors in the MGM solutions. Empirically derived values for these proportionality coefficients are $C_1 = 3.19 \times 10^{-3}$, $C_2 = 1.45 \times 10^{-3}$, $C_3 = 3.10 \times 10^{-3}$, $C_4 = 7.20 \times 10^{-3}$, and $C_5 = -4.69 \times 10^{-2}$ with a root mean square error of 0.11 ions. Actual and predicted Fe^{2+} pfu using this relationship are presented in Table 5 and illustrated in Figure 6a. Similar equation relating the Mg/Fe ratio to band areas can also be established. Empirically derived proportionality coefficients for the Mg# $[X_{Mg}/(X_{Mg} + X_{Fe})]$ are $C_1 = 2.9 \times 10^{-5}$, $C_2 = 4.72 \times 10^{-4}$, $C_3 = 3.87 \times 10^{-4}$, $C_4 = 1.65 \times 10^{-3}$, and $C_5 = 1.007$ with a root mean square error of 0.024, and the results are presented in Table 5 and Figure 6b.

The systematic nature of the MGM solutions and the relationship of bands to known absorptions indicate the MGM shows significant promise as a method for decon-

volving complex overlapping absorption bands in reflectance spectra. Ultimately it may be possible to associate particular bands with site occupancies. The high correlation between predicted and actual Mg# and Fe^{2+} pfu shows that the MGM can be used as a high-quality tool for remote compositional analysis and can provide nondestructive estimates of mineral composition in laboratory applications.

OH overtones

Burns and Strens (1966) established the geochemical and crystallographic origin of four OH^- stretching fundamentals in Fe-Mg ortho- and clinoamphiboles. The proportion of Fe^{2+} and Mg in the M1 and M3 sites determines the band positions of the fundamental stretching bands. Using transmission spectra, Burns and Strens (1966) also established a relationship between the relative strengths of the bands and proportional concentration of Fe^{2+} and Mg in the M1 and M3 sites. These relationships

TABLE 5. Actual and calculated Fe^{2+} pfu and Mg numbers

Sample	1	2	4	5	6	7	8	9	10	11	12	13	17	18	19	20	21	9a	9g
							Fe^{2+} pfu from electronic absorptions												
Act	0.43	0.46	0.40	0.54	0.28	0.66	0.86	0.30	0.63	0.62	0.27	0.47	0.67	0.54	0.49	2.39	2.51	0.63	0.57
Calc	0.54	0.61	0.47	0.54	0.34	0.40	1.02	0.21	0.78	0.68	0.34	0.36	0.45	0.51	0.45	2.35	2.45	0.61	0.62
Correlation coefficient = 0.9825																			
							Mg number from electronic absorptions												
Act	0.86	0.87	0.86	0.88	0.93	0.85	0.74	0.93	0.86	0.86	0.94	0.88	0.85	0.88	0.86	0.47	0.39	0.87	0.87
Calc	0.86	0.84	0.87	0.87	0.93	0.90	0.75	0.94	0.81	0.83	0.91	0.91	0.87	0.87	0.88	0.45	0.42	0.88	0.87
Correlation coefficient = 0.9854																			
							Mg number from OH overtone absorptions												
Act	0.86	0.87	0.86	0.88	0.93	0.85	0.74	0.93	0.86	0.86	0.94	0.88	0.85	0.88	0.86	0.47	0.39	0.87	0.87
Calc	0.78	0.78	0.78	0.78	0.84	0.77	0.66	0.85	0.78	0.77	0.85	0.80	0.76	0.71	0.82	0.40	0.36	0.84	0.82
Correlation coefficient = 0.9808																			

are

$$\Sigma\ Fe^{2+}(M1,M3) = 1B' + 2C' + 3D'$$
$$\Sigma\ Mg^{2+}(M1,M3) = 3A' + 2B' + 1C'$$

where A', B', C', and D' are the relative strengths of each band, normalizing the sum of the strengths to 1.0. It follows that an estimate of the Mg# can be obtained by

$$Mg\# = (3A' + 2B' + C')/3.0.$$

For this relationship to be an accurate representation of the true Mg#, ion distribution must be random and contributions to the intensity of the fundamental absorptions must be primarily from Fe^{2+} and Mg (Strens, 1974; Law, 1976). These principles will be applied to the data presented in Figure 1b using the MGM to determine the strengths of the four bands. The analysis of Burns and Strens (1966) and most subsequent applications of the relationship have used transmission data obtained in the wavelength region of the fundamental stretching absorption (2.7–2.8 μm). Presented here is one of the few applications of this technique to high-resolution reflectance spectra measured of the overtone absorptions near 1.4 μm.

The Mg#'s calculated using the strengths of absorptions *A, B,* and *C* determined with the MGM model are presented in Table 5 and Figure 7 along with the Mg# determined from chemical analyses. These calculated Mg#'s have a correlation coefficient of 0.971 with the actual Mg#. The samples that plot away from the highly correlated grouping are readily explained from site population arguments. Samples 9a and 9g have higher Mg#'s because they have a large proportion of available Fe^{2+} in the M4 site and therefore less in the M1 and M3 sites. Sample 18 has a lower than expected Mg# because there is no Fe^{2+} in the M4 site and therefore more Fe^{2+} available for the M1 and M3 sites. These samples violate the assumption that the ions of Fe^{2+} and Mg are randomly distributed in the M sites.

The calculated Mg#'s underestimate the Mg#'s determined analytically. Wilkens (1970), Strens (1974), and Clark et al. (1990) all observed a systematic overestimation of the amount of Fe^{2+} in the M1 and M3 sites in similar analyses. The simplest explanation is that in calcic amphiboles Fe^{2+} is much more abundant in the M1 and M3 sites because Ca fills the M4 site and Fe^{2+} avoids the M2 site. However the amount of Fe^{2+} predicted in the M1 and M3 sites exceeds the total amount of Fe^{2+} in some samples. Clark et al. (1990) postulate that the effects of multiple scattering increase the apparent depths of weak bands relative to strong bands, thereby skewing the calculations toward lower Mg# estimates. This hypothesis predicts that estimates of Mg#'s for samples with high Fe should be overestimated. This is not the case, as samples 20 and 21 follow the same trend as the low-Fe samples.

It is observed that samples with higher Fe also have steeper spectral slopes toward longer wavelengths near 1.4 μm (Fig. 1a, Table 1), caused by the long wavelength wings of Fe^{2+} electronic transition absorptions. This es-
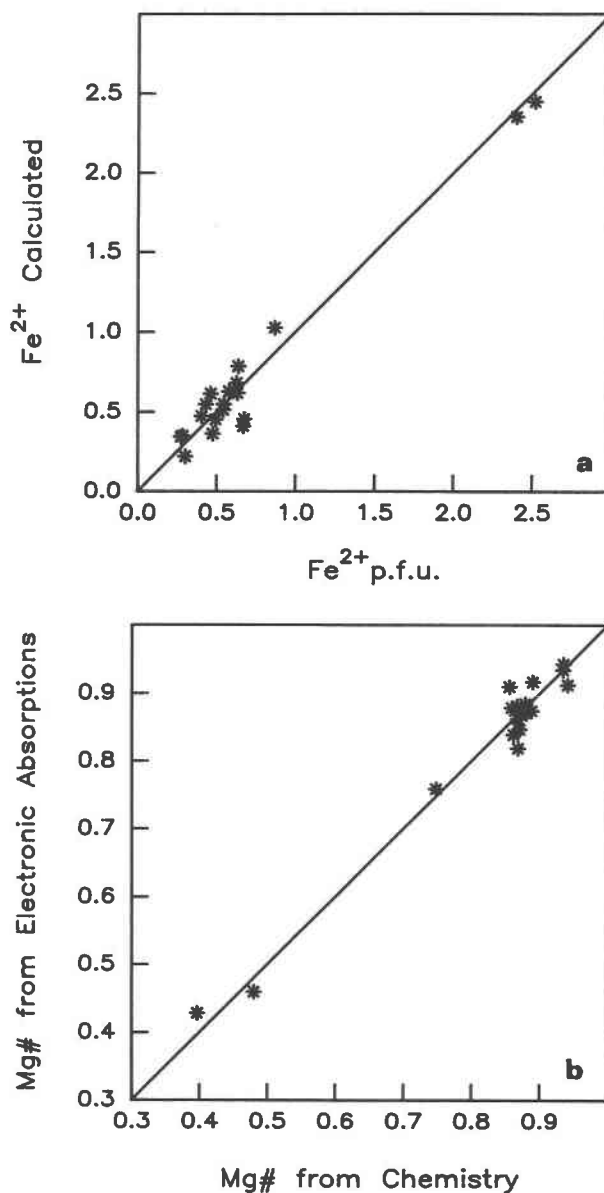

Fig. 6. Estimates of Fe content and Mg/Fe ratios in the actinolite samples from the area of absorption. (**a**) Amount of Fe^{2+} pfu determined analytically and plotted against the amount of Fe^{2+} (calculated) predicted from a linear combination of the areas of the model bands 3, 4, 5, and 6. (**b**) Mg# determined analytically and plotted against the Mg# (calculated) predicted from a linear combination of the areas of the model bands 3, 4, 5, and 6. The values used to create these plots are given in Table 5. The solid line in each plot indicates a 1:1 correlation.

sentially reduces the apparent strength of the Mg-OH relative to the Fe-OH absorptions. A similar effect can be seen in the strengths of the combination overtone bands in the wavelength region of 2.2–2.4 μm, where samples with the strong 2.4-μm electronic transition bands (samples 9a, 9g, 13) have the weak combination overtone bands relative to samples with weak 2.4-μm electronic absorp-
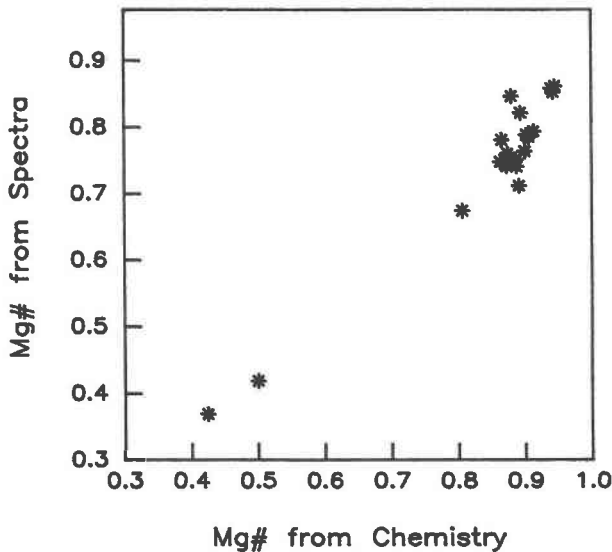
Fig. 7. Mg# determined analytically and plotted against the Mg# predicted using the techniques of Burns and Strens (1966) on the first overtone of the OH stretching fundamental. The values used to create this plot are given in Table 5.
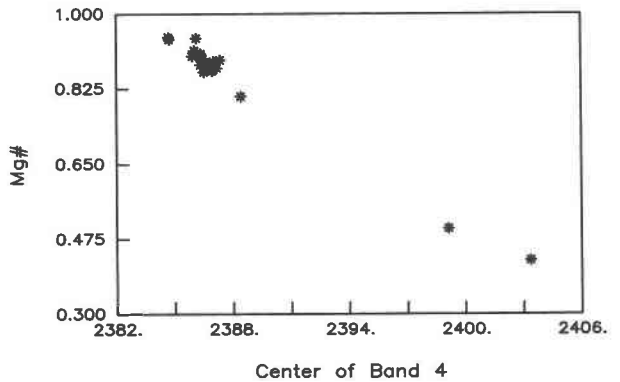

Fig. 8. The center of band 4 plotted against the Mg# determined analytically. The position of this band is a sensitive indicator of Fe/Mg ratios for tremolite-actinolite solid solution.

tions (samples 9, 12, 18). Even though the Mg bands are enhanced by multiple scattering, as the amount of Fe increases the increase in slope decreases the relative strength of these bands. Therefore even the predicted values for high-Fe samples are too low.

Combination overtones

The association between the OH combination overtone bands positioned between 2.2 and 2.5 μm and composition is less well understood than the stretching fundamentals and overtones. These bands are thought to be combination overtones involving the metal-OH$^-$ bending modes centered near 650 cm^{-1} and the OH$^-$ stretching modes centered near 3750 cm^{-1} (Hunt, 1977). From Figure 1c, three well-resolved band minima and a shoulder near 2.26 μm, indicating the presence of a fourth band, are observed in all spectra. Minor bands of variable intensity and importance occur near 2.25 μm, 2.35 μm, and at wavelengths longer than 2.4 μm. Variations in band strength are due primarily to the relatively intensity of the 2.4-μm electronic transition band (e.g., samples 9a and 9g have the strongest 2.4-μm electronic absorption bands and the weakest combination overtone bands). The vibrational bands become broader and the band minima move to longer wavelengths with increasing Fe.

Correlations of the model parameters with composition were computed, and it was found that the positions of bands 2, 3, and 4 were most strongly correlated with the Fe/Mg ratios and the total amount of Fe^{2+}. Band 4 is the most highly correlated with the Fe/Mg ratios, and a plot of the position of band 4 against the Mg# determined from chemical analysis is presented in Figure 8. The other bands may be as highly correlated with the Mg#, but since

there is a high degree of overlap between these bands, there is a greater uncertainty in the band position determined by the model. Band 4, however, is not affected by the complications of overlapping bands, and the position of this band models a very sensitive indicator of the Fe/Mg ratios in these samples.

The position of band 4 shifts approximately 40 cm^{-1} from low Fe (sample 12) to high Fe (sample 20). Barabanov et al. (1974) document a shift of approximately 10–15 cm^{-1} across a comparable compositional range in the position of fundamental bending mode minima. The remaining 25–30 cm^{-1} is contributed by the difference in wavelength between the dominant stretching mode absorption in low-Fe samples (A) and high-Fe samples (C). A continuous rather than discrete shift in band position is observed because contributions from individual stretching modes are not resolved with the sampling resolution used to acquire these data.

The width of band 4 increases from approximately 80 cm^{-1} in sample 12 to 130 cm^{-1} in sample 21 for a total increase of about 50 cm^{-1}. Analyses of fundamental vibrational absorptions (Burns and Greaves, 1971; Barabanov et al. 1974) and of the 1.4-μm overtone bands in this study indicate no systematic changes in band widths with changing compositions. However, the difference between the wavelength positions of the wings of the combined absorptions in the 1.4-μm region for samples 12 and 21 is also approximately 50 cm^{-1}. Therefore the increase in width of the combination overtones is simply a consequence of the increase in the relative strength of the FeFeMg and FeFeFe stretching fundamentals and of the fact that individual overtones of the stretching fundamentals are not resolved with 2-nm spectral resolution used to acquire these data.

Therefore, the majority of the systematic changes in absorption width and band positions are contributed by the well-understood changes in number and relative strength of fundamental bending mode vibrations. Two simple predictions can be made based on this result: the width of the combination overtone absorptions will nar-

row and band positions will continue to shift to longer wavelengths as the Mg#'s of samples progress to zero.

Discussion and conclusions

The reflectance spectra of the minerals studied here reflect the flexibility of the amphibole crystal structure. This structure can accommodate a wide range of compositions in many different ordering and site-population configurations, even in minerals of the relatively simple tremolite-actinolite-ferroactinolite solid solution series examined in this analysis. Nevertheless the results of the MGM model applied to reflectance spectra of these minerals indicate that many of the complexities observed in these data can be examined through quantitative analysis of reflectance spectra. The number and position of the bands required to model features thought to be due to electronic transitions and charge transfers correspond well with previous work on oriented crystal transmission spectra of similar minerals. For the analyses of the OH overtone absorption in reflectance spectra it was found that the MGM model provided a constrained and consistent tool to quantify the systematic variations in these absorptions with chemistry.

Analysis of the areas of individual model electronic absorption bands with composition indicates that no one band is a sensitive measure of the bulk composition of these samples. Because absorptions in the wavelength region examined are primarily due to Fe^{3+} and Fe^{2+}, most of the individual bands exhibit weak linear relationships between area and the amount of Fe^{2+}, whereas the total area of all bands thought to be associated with electronic transitions show a relatively high linear correlation with the total amount of Fe^{2+} in these samples. Because these model bands are expected to have different proportionality constants to composition, variability in site occupancy is anticipated to cause scatter in the simple relationships between band area and composition. Therefore a simple linear relationship was established to relate band area of bands 3, 4, 5, and 6 to the amount of Fe^{2+} pfu and the Mg# using different proportionality constants for each band. This relationship provides a reasonably accurate estimate of the Fe content of the samples, especially for applications to remote observations. It is likely that this relationship could be strengthened with increased knowledge of actual site occupancy or refined calculations to take variable site occupancy into account.

The application of the MGM to the OH overtone and combination overtone bands provides a useful tool to quantify the systematic variations in band strength and position associated with chemical change. The method developed by Burns and Strens (1966) was used to calculate the proportion of Mg and Fe^{2+} in the M1 and M3 sites and also the Mg#. This application is one of the few to use reflectance spectra of the first overtone of the OH stretching fundamental to characterize the relative strengths of these bands. It was found that the MGM provided a self-consistent estimate of the Mg# when an additional band was included in the analysis to account for absorptions due to adsorbed H_2O. Although the actual Mg# is systematically greater than the calculated Mg#, this approach is nondestructive, requires little sample preparation, and can be corrected simply for the systematic difference between the actual and calculated Mg#'s. It must be noted, however, that this method has only been tested on simple chemical systems. The presence of appreciable amounts of Al^{3+} and Fe^{3+} in the M1 and M3 sites, or Na and K in the A sites, results in an increase in the number or position of the stretching fundamentals (Burns and Greaves, 1971). These absorptions overlap significantly with the $(Mg,Fe)-OH^-$ absorptions. However, the stretching fundamentals exhibit very low variability in model band positions and widths. Through the use of strict mathematical constraints on allowable band widths and positions, the difficulties of overlapping and superimposed absorptions in complex systems could be addressed.

Results from the application of the MGM to the combination overtone bands indicate that the positions of these bands are sensitive indicators of the Fe/Mg ratios of the minerals. It was found that the positions of the model bands move to longer wavelengths and the widths of the bands increase with increasing Fe^{2+} content. The position of the band centered near 2.4 μm is the most highly correlated with the Fe/Mg ratios of the samples, partly because this band is isolated and model solutions are better constrained. Both the broadening of the absorptions with increasing Fe and the shift in wavelength position are a function of the increased contributions of the C and D stretching fundamentals to the combination overtones. The stretching fundamentals are too closely spaced to be resolved in the combination overtones, but the increased importance of the Fe-OH bands is still observed.

REFERENCES CITED

Adams, J.B. (1974) Visible and near-infrared diffuse reflectance: Spectra of pyroxenes as applied to remote sensing of solid objects in the solar system. Journal of Geophysical Research, 79, 4829–4836.

Allen, G.C., and Hush N.S. (1967) Intervalence-transfer absorption. Part 1. Qualitative evidence for intervalence-transfer absorption in inorganic systems in solution and in the solid state. In F.A. Cotton, Ed., Programs in Inorganic Chemistry, vol. 8, p. 357–389. Wiley, New York.

Bancroft, G.M., and Burns, R.G. (1969) Mössbauer and absorption spectral study of alkali amphiboles. Mineralogical Society of America Special Paper, 2, 137–148.

Barabanov, A.V., Zorina, M.L., and Sobolev, V.K. (1974) Infrared spectra

of amphiboles from metamorphic rocks. Material Mineralov Kol'skivskaya Polenostrova, 10, 165–175.

Burns, R.G. (1970) Mineralogical application to crystal field theory, 224 p. Cambridge University Press, London.

Burns, R.G., and Greaves C. (1971) Correlations of infrared and Mössbauer site population measurements of actinolites. American Mineralogist 56, 2010–2032.

Burns, R.G., and Prentice F.J. (1968) Distribution of iron cations in the crocidolite structure. American Mineralogist, 53, 770–776.

Burns, R.G., and Strens, R.G.J. (1966) Infrared study of the hydroxyl bands in clinoamphiboles. Science, 153, 9:890–892.

Clark, R.N. (1981) Water frost and ice: The near-infrared spectral reflectance 0.65–2.5 μm. Journal of Geophysical Research, 86, 3087–3096.

Clark, R.N., King, T.V.V., Klejwa, M., Swayze, G.A., and Vergo N. (1990) High spectral resolution reflectance spectroscopy of minerals. Journal of Geophysical Research, 95, 12653–12680.

Ernst, W.G., and Wai C.M. (1970) Mössbauer, infrared, and optical study of cation ordering and dehydrogenation in natural and heat treated sodic amphiboles. American Mineralogist 55, 1226–1258.

Farmer, V.C., Ed. (1974) The infrared spectra of minerals, 539 p. The Mineralogical Society, London.

Farr, T.G., Bates, B.A., Ralph, R.L., and Adams, J.B. (1980) Effects of overlapping optical absorption bands of pyroxene and glass on the reflectance spectra of lunar soils. Proceedings of the 11th Lunar and Planetary Science Conference, 719–729.

Ghose, S. (1961) The crystal structure of cummingtonite. Acta Crystallographica, 14, 622–627.

Goldman, D.A., and Rossman, G.R. (1977) The identification of Fe^{2+} in the $M(4)$ site of calcic amphiboles. American Mineralogist, 62, 205–216.

Gwinn, R., and Hess, P.C. (1989) Iron and titanium solution properties in peraluminous and peralkaline rhyolitic liquids. Contributions to Mineralogy and Petrology, 101, 326–338.

Hawthorne, F.C. (1981) Amphibole spectroscopy. In Mineralogical Society of America Reviews in Mineralogy, 9A, 103–140.

——— (1983) The crystal chemistry of amphiboles: A review. Canadian Mineralogist, 21, 173–480.

Hazen, R.M., Mao, H.K., and Bell, P.M. (1977) Effects of compositional variation on absorption spectra of lunar olivines. Proceedings of the Eighth Lunar Science Conference, 1081–1090.

Hazen, R.M., Bell, P.M., and Mao, H.K. (1978) Effects of compositional variation on absorption spectra of lunar pyroxenes. Proceedings of the Ninth Lunar and Planetary Science Conference, 2919–2934.

Huguenin, R.L., and Jones J.L. (1986) Intelligent information extraction from reflectance spectra: Absorption band positions. Journal of Geophysical Research, 91, 9585–9598.

Hunt, G.R. (1977) Spectral signatures of particulate minerals in the visible and near-infrared. Geophysics, 42, 501–513.

Kaper, H.G., Smits, D.W., Schwarz, U., Takakuba, K., and Van Woerden, H. (1966) Computer analysis of observed distributions into Gaussian components. Bulletin of the Astronomical Institute of the Netherlands, 18, 465–487.

King, T.V.V., and Ridley, W.I. (1987) Relation of the spectroscopic reflectance of olivine to mineral chemistry and some remote sensing implications. Journal of Geophysical Research, 92, 11457–11469.

Kukovskii, E.G., and Litvin A.L. (1970) Infrared spectra of amphiboles. Konstitutsiia i Sviostva Mineralov, 58, 81–85.

Laird, J., and Albee, A.L. (1981) Pressure, temperature, and time indicators in mafic schist: Their application to reconstructing the polymetamorphic history of Vermont. American Journal of Science, 281, 127–175.

Law, A.D. (1976) A model for the investigation of hydroxyl spectra of amphiboles. In R.G.J. Strens, Ed., Physics and chemistry of minerals and rocks, p. 677–686. NATO Advanced Study Institute, Wiley, New York.

Marfunin, A.S. (1979) Physics of minerals and inorganic materials, 340 p. Springer-Verlag, New York.

McCord, T.B., Clark, R.N., and Singer, R.B. (1982) Mars: Near-infrared reflectance spectra of surface regions and compositional implications. Journal of Geophysical Research, 87, 3021–3032.

Mitchell, J.T., Bloss, F.D., and Gibbs, G.V. (1970) A refinement of the structure of actinolite. American Mineralogist, 55, 302–303.

Mueller, R.G. (1960) Compositional characteristics and equilibrium relationships in mineral assemblages of a metamorphosed iron formation. American Journal of Science, 258, 449–497.

Mustard, J.F. (1991) Spectral modelling of the unknown: An example using talc and actinolite (abs.). Lunar and Planetary Science, 22, 949–950.

Mustard, J.F., and Pieters, C.M. (1989) Photometric phase functions of common geologic minerals and applications to quantitative analysis of mineral mixture reflectance spectra. Journal of Geophysical Research, 94, 13619–13634.

Pieters, C.M. (1983) Strength of mineral absorption features in the transmitted component of near-infrared reflected light: First results from RELAB. Journal of Geophysical Research, 88, 9534–9544.

——— (1986) Composition of the lunar highland crust from near-infrared spectroscopy. Reviews of Geophysics, 24, 557–578.

Robinson, P., Spear F.S., Schumacher, J.C., Laird, J., Klein, C., Evans, B.W., and Doolan, B.L. (1982) Phase relations of metamorphic amphiboles: Natural occurrence and theory. In Mineralogical Society of America Reviews in Mineralogy, 9B, 1–228.

Roush, T.L., and Singer, R.B. (1986) Gaussian analysis of temperature effects on the reflectance spectra of mafic minerals in the 1.0 micron region. Journal of Geophysical Research, 91, 10301–10308.

Skogby, H., and Annersten, H. (1985) Temperature dependent Mg-Fe-cation distribution in actinolite-tremolite, Neues Jahrbuch für Mineralogie Monatshefte, 13, 193–203.

Skoog, D.A., and West, D.M. (1982) Fundamentals of analytical chemistry, p. 39–90. CBS College Publishing, New York.

Smith, G., and Strens, R.G.J. (1976) Intervalence transfer absorption in some silicate, oxide and phosphate minerals. In R.G.J. Strens, Ed., Physics and chemistry of minerals and rocks, p. 583–612. NATO Advanced Study Institute, Wiley, New York.

Strens, R.G.J. (1974) The common chain, ribbon, and ring silicates, In V.C. Farmer, Ed., The infrared spectra of minerals, p. 305–330. Mineralogical Society of London, London.

Sunshine, J.M., and Pieters, C.M. (1990) Extraction of compositional information from olivine reflectance spectra: A new capability for lunar exploration (abs.). Lunar and Planetary Science, 21, 1223–1224.

——— (1991) Identification of modal abundances in the spectra of natural and laboratory pyroxene mixtures: A key component for remote analysis of lunar basalts (abs.). Lunar and Planetary Science, 22, 1361–1362.

Sunshine, J.M., Pieters, C.M., and Pratt, S.F. (1990) Deconvolution of mineral absorption bands: An improved approach. Journal of Geophysical Research, 95, 6955–6966.

Thornber, C.R., Roeder, P.L., and Foster, J.R. (1980) The effect of composition on the ferric-ferrous ratio in basaltic liquids at atmospheric pressure. Geochemical et Cosmochimica Acta, 44, 525–532.

Weidner, V.R., and Hsia, J.J. (1981) Reflection of pressed polytetrafluoroethylene powder. Journal of the Optical Society of America, 71, 856–861.

White, W.B., and Keester, K.L. (1967) Selection rules and assignments for the spectra of ferrous iron in pyroxenes. American Mineralogist, 52, 1508–1514.

Wilkens, R.W.T. (1970) Iron-magnesium distribution in the tremolite-actinolite series. American Mineralogist, 55, 1992–1998.

Wilkens, R.W.T., Davidson, L.R., and Ross, J.R. (1970) Occurrence and infrared spectra of holmquistite and hornblende from Mt. Marion, near Kalgoorlie, Western Australia. Contributions to Mineralogy and Petrology, 28, 280–287.